Optics Letters

Fast photoacoustic-guided depth-resolved Raman spectroscopy: a feasibility study

Fei Gao,[1,†] Yi Hong Ong,[2,†] Gaoming Li,[1,3] Xiaohua Feng,[1] Quan Liu,[2] and Yuanjin Zheng[1,*]

[1]School of Electrical and Electronic Engineering Nanyang Technological University, 50 Nanyang Avenue, Singapore 639798, Singapore
[2]School of Chemical and Biomedical Engineering, Nanyang Technological University, 70 Nanyang Drive, Singapore 637457, Singapore
[3]Fujian Normal University, Key Laboratory of OptoElectronic Science and Technology for Medicine, Ministry of Education, Fuzhou 350007, China
*Corresponding author: yjzheng@ntu.edu.sg

Received 16 April 2015; revised 14 June 2015; accepted 8 July 2015; posted 10 July 2015 (Doc. ID 238190); published 27 July 2015

In this Letter, photoacoustic-guided Raman spectroscopy (PARS) is proposed for a fast depth-resolved Raman measurement with accurate depth localization. The approach was experimentally demonstrated to receive both photoacoustic and Raman signals from a three-layer agar phantom based on a developed synergic photoacoustic-Raman probe, showing strong depth correlation and achieving magnitude of faster operation speed due to photoacoustic time-of-flight measurement and guidance, compared with the conventional depth-resolved Raman spectroscopy method. In addition, further combination with advanced optical-focusing techniques in biological-scattering medium could potentially enable the proposed approach for cancer diagnostics with both tight and fast optical focusing at the desired depth of tumor. © 2015 Optical Society of America

OCIS codes: (110.5125) Photoacoustics; (170.5660) Raman spectroscopy; (110.0113) Imaging through turbid media.

http://dx.doi.org/10.1364/OL.40.003568

Raman spectroscopy is a bond-selective spectroscopic technique based on inelastic scattering of light. It exhibits high chemical specificity and can quickly provide information on the molecular composition of a sample without labeling [1]. To further advance this technology for deep-tissue measurement, depth-sensitive techniques such as confocal Raman microspectroscopy [2], Kerr-gated time-resolved Raman spectroscopy [3,4], and spatially offset Raman spectroscopy [5] have been studied extensively in recent years to extract depth specific chemical/diagnostic information from diffusively scattering samples. Confocal Raman microspectroscopy is highly preferable in various biomedical applications due to its superior spatial resolution in imaging of tissue samples. However, without prior depth information of a subsurface target, the light source has to be gradually scanned through the entire sample to locate the region of interest, rendering this technique highly inconvenient and time-consuming. Moreover, due to the strong scattering of biological tissue, the optical focusing in deep tissue is not ideal and strongly diffused, which impairs accurate localization of the sample. Therefore, it is highly expected that if the prior depth information of the sample is available, the focusing of the light will be much faster and more efficient with higher localization accuracy.

Photo-acoustic (PA) sensing and imaging techniques have attracted tremendous research interest in recent years due to its breakthrough of optical diffusion limit by ultrasound detection [6,7]. Through optical absorption and thermo-elastic expansion, PA signal is generated and detected by contact ultrasound transducers or noncontact laser interferometry/vibrometer methods. PA technique could readily provide depth information by the time-of-flight measurement of the PA signal for accurate localization, which enables 3D deep-tissue imaging [8,9]. Functional PA techniques are also available by exploring the optical absorption spectrum of both endogenous and exogenous absorbers using multi-wavelength laser source for oxygen saturation and lipid detection, etc. [10–13]. However, the specificity of the optical absorption is poor compared to the bond-selective Raman spectroscopy mentioned above. Therefore, a synergic integration of PA technique and Raman spectroscopy is highly demanded to deliver bond-selective specificity with fast and accurate depth localization for tissue characterization. A recent study on stimulated Raman PA imaging has proved the significant potential of combining PA and Raman, which however still suffers weak PA-signal generation efficiency [14,15].

In this Letter, we propose a PA-guided depth-resolved Raman-spectroscopy (PARS) technique to fully utilize the merits of both techniques for bond-selective specificity tissue characterization with fast and accurate depth localization. Both PA signals and Raman-scattered photons from the same sample are collected concurrently to show high correlation with depth. Fast and accurate light focusing inside the sample is achieved for depth-resolved Raman-spectroscopic analysis with the help of PA localization. The proposed technique is also potentially applicable to other optical measurements, such as diffuse reflectance or fluorescence measurements.

We designed and constructed a confocal PA-Raman probe as shown in Fig. 1(a). The PA system and Raman system shared

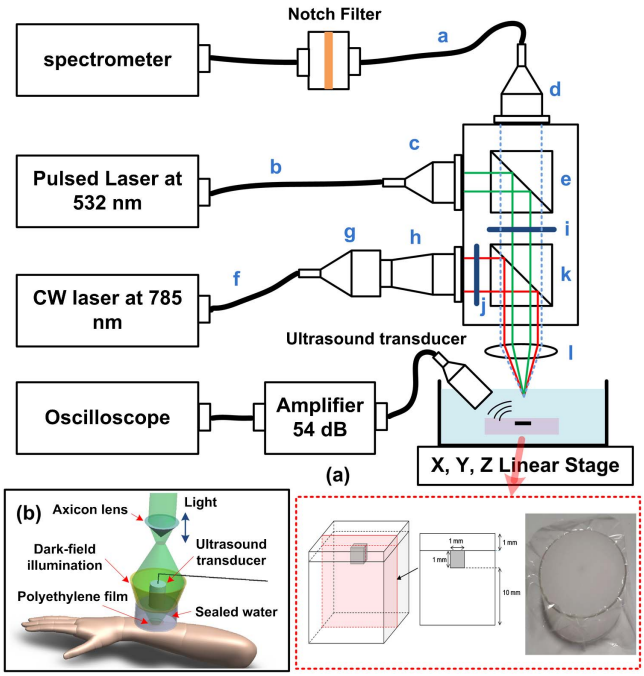

Fig. 1. (a) Experimental setup of the PA-guided Raman probe and the phantom structure. a = collection fiber, multimode, 400 μm, NA = 0.22; b = 532 nm excitation fiber; c = collimator including convex lens, FL = 35 mm; d = collimator with convex lens, FL = 35 mm; e = 532 nm beam splitter, 50R/50T; f = excitation fiber, multimode, 100 μm, 0.22NA; g = 785 nm collimator; h = beam expander; i = longpass filter (Semrock, Part Number: LP02-785RU-25); j = 785 nm bandpass filter (Semrock, Part Number: LD01-785/10-25); k = 785 nm beam splitter dichroic mirror (Semrock, Part Number: LPD01-785RS-25); l = convex lens, FL = 50 mm. (b) An envisioned *in vivo* application scheme of the proposed PA-Raman probe with dark-field light illumination configuration.

the same optical focusing lens with both excitation lasers focused at the same focal point. This ensures that the collected PA signal and Raman signal are emitted from the same location of the sample, and makes it possible to use the real-time PA signal to guide the Raman signal detection. The water tank was mounted on a XYZ translation stage, which has a 26-mm translation range in each axis. The excitation source for PA signal generation was a Q-switched pulsed laser (FDSS 532-1000, CryLas, GmbH) with wavelength of 532 nm and pulse width of 1.8 ns. The output of the laser was coupled to a multimode fiber with a diameter of 100 μm and a numerical aperture of 0.22. PA signal was collected by a wideband ultrasound transducer with 5-MHz central frequency (V326-SU, Olympus), followed by an ultrasound preamplifier with 54-dB gain (Model 5662, Olympus). A digital oscilloscope was used to record the photo-acoustic signal at 500-MHz sampling rate. During the PA measurements, the 785-nm dichroic mirror and the longpass filter were removed from the setup to allow the 532-nm excitation light to pass through. Fiber "f" was connected to an infrared diode-laser module (FC-D-785, CNI Optoelectronics Tech. Co. Ltd., Changchun, P.R. China) with a maximum output power of 500 mW at 785 nm. The Raman signals collected by fiber "a" were coupled to a 303-mm focal length, motorized, Czerny–Turner spectrograph (Shamrock 303, Andor Technology, Belfast, UK) equipped with a 1200-line/mm grating (SR3-GRT-1200-1000, Andor Technology, Belfast, UK) and a research-grade CCD (DU920P-BR-DD, Andor Technology, Belfast, UK), which yielded a spectral resolution of 0.07 nm. The acquisition time for each Raman spectrum was 5 s. The power of 785-nm laser measured on sample surface was 75 mW. An envisioned *in vivo* application is shown in Fig. 1(b), where optical illumination and ultrasound detection are confocally aligned, providing more accurate depth estimation. Meanwhile, optical focusing spot could be easily tuned by moving the axicon lens vertically, without interfering ultrasound detection.

A three-layer phantom was fabricated for the proof-of-concept study. A highly purified agarose powder (Vivantis, California, USA) was added into distilled water at a concentration of 1% w/w. The mixture was brought to a boil using a microwave oven until the agarose powder melted and dissolved completely. Then the agar solution was poured into a mold and left for cooling at room temperature until it was set. A three-layered agar phantom was prepared, in which a small phantom cube with trans-Stilbene powder (Sigma-Aldrich, Missouri, USA) was sandwiched between the two agar layers with a dimension of 1 mm × 1 mm × 1 mm. The thickness of the top layer was 1 mm, and the thickness of bottom layer was 10 mm, whereas the lateral dimension of both layers was made greater than 10 mm in diameter to represent a semi-infinite medium. Intralipid 20% (Fresenius Kabi, Bad Homburg, Germany) was added into each layer at a different concentration to mimic the light-scattering properties of the epidermis and dermis of normal human skin so that the reduced scattering coefficient, μ_s', matched the published value in [16]. Nigrosin dye was added to the trans-Stilbene powder layer, to reach a final concentration of 0.1 mg/ml, to enhance the PA signal contrast of the middle layer from the top and bottom layers. The absorption coefficients of 0.1-mg/ml nigrosin solution at the excitation wavelengths of 532 nm and 785 nm were measured to be 4.07 cm^{-1} and 1.76 cm^{-1}, respectively, using a UV–VIS spectrophotometer (UV-2450, Shimadzu Corp., Kyoto, Japan). A piece of plastic wrap was placed between any two adjacent layers to prevent the diffusion of Nigrosin into the top and bottom layers.

Preliminary experiments on the PA-guided depth-resolved Raman spectroscopy were conducted using the fabricated three-layer tissue-mimicking phantom. In the first experiment to prove the trend of PA-Raman correlation, the focusing spot of the PA-Raman probe was scanned by 26 mm in depth gradually from top to bottom with a step size of roughly 2 mm to prove the strong correlation between the PA and Raman signals. As shown in Fig. 2, when the laser focal point was scanned from location 0 mm down to 26 mm in the depth direction, the amplitudes of both PA waveform [Fig. 2(a)] and Raman peak intensity [Fig. 2(b)] at a Raman shift of 1485 cm^{-1} experienced strong correlation with about 2-mm shift due to the diffusion of the Nigrosin dye toward the bottom layer. It also worked for another two Raman shift of 1075 and 1525 cm^{-1} (not shown here), i.e., both amplitudes were increasing and then decreasing

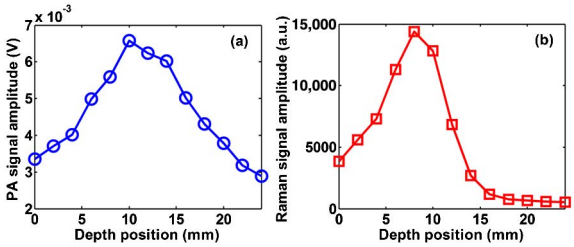

Fig. 2. (a) Amplitude of the PA signal recorded at different depth positions. (b) Amplitude of the Raman signal of 1485 cm^{-1} wavenumber shift recorded at different depth positions.

caused by the focal point scanned across the phantom. The correlation factors for these three Raman shift are 0.87, 0.87, and 0.86, respectively (data at 26 mm is discarded). This motivated us to use PA signal as a guide for depth-resolved Raman spectroscopy by utilizing their strong correlation in depth due to the reason that the middle layer exhibits both strong Raman scattering and photo-acoustic generation. From Fig. 2, the maximum signal strength occurred in the range of 8–10 mm. However, it is worth noting that if the depth information accuracy of 0.1 mm is required, 80–100 scanning steps just for one directional scanning will be needed to reach the maximum responses of Raman signals, which is quite time-consuming and inconvenient. To utilize the time-of-flight measurement of PA signals as prior depth information, an expedited focusing with much less scanning steps could be achieved, which is experimentally demonstrated next.

In the second experiment, the prior depth information extracted from the time-of-flight measurements of PA signals was used to guide the optical focusing for obtaining maximum Raman signals in a much faster way. Before the measurement, raster scanning of the PA-Raman probe in x–y coordinates could be performed to determine the location of the target, where maximum PA signal's amplitude and minimum PA signal arrival delay can be observed. The operation procedure included several iterative steps:

(1) Both the optical focal point and the unfocused ultrasound transducer were positioned at d1 = 0 mm with a fixed ultrasound detection angle, such as 30°, in this experiment as shown in Fig. 3(a), where d1 = 0 mm is the baseline, d2, d3, and d4 are the estimated depth position relative to the baseline. PA measurement was performed first to find the updated depth d2 information of the phantom by time-of-flight calculation $d2 = c \times t1 \times \sin(30°) = 0.5 \times c \times t1$, where c is the acoustic speed (1500 m/s), and t1 is the PA signal propagation time from the phantom's illumination spot to the transducer surface when the focal point is d1. Meanwhile, the Raman spectrum at position d1 mm was recorded [Fig. 3(a)].

(2) Iteratively, the optical focal point was steered to position d2 for PA measurement to get an updated position d3, and so on [Figs. 3(b) and 3(c)]. Finally, the depth information will be converged to $d_n = d_{n-1}$ with required accuracy, e.g., 0.1 mm, which could be well differentiated by time-of-flight measurement of the PA signal's profile from a 5-MHz transducer (with maximum frequency around 10 MHz) without sacrificing the detection sensitivity.

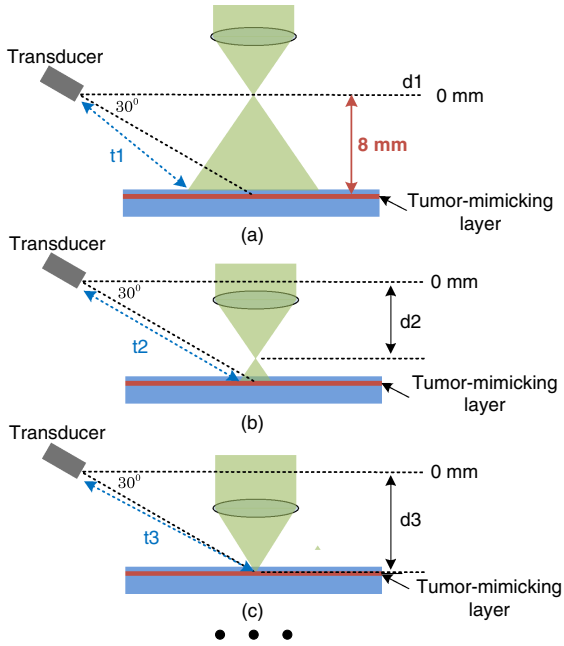

Fig. 3. PA-guided optical focusing procedure iteratively for depth-resolved Raman measurement of depth positions at (a) d1 = 0 mm, (b) d2, (c) d3, and more.

The underlying reason why this approach can work is: at each scanning step, it gives better optical focusing on the phantom, and thereafter generates sharper and stronger PA signal waveform, which consequently renders more-accurate time-of-flight calculation and estimation of depth information of the phantom. Therefore, after several rounds of iteration, the PA signal will reach maximum amplitude and provide updated depth estimation, which is sufficiently accurate and close to the real targeted focal depth. Meanwhile, the Raman spectrum will also be maximized and specific to the focal depth.

As predicted by the PA-guided depth-resolved Raman spectroscopy technique described above, the measurement results in Fig. 4 verified the feasibility of the approach very well by placing the phantom 8 mm in depth. In Fig. 4(a), the first time-of-flight measurement of PA signal peak at t1 = 9.4 μs gave the predicted depth information of d2 = 7.0 mm. The corresponding Raman spectrum was shown in Fig. 4(b). Then the optical focal point was steered to position d2 by the translation stage. As shown in Fig. 4(c), the second time-of-flight measurement of PA signal peak at t2 = 10.8 μs gave the improved predicted depth information of d3 = 8.1 mm with higher accuracy. The corresponding Raman spectrum was shown in Fig. 4(d). Further, the focal point was steered to position d3 by the translation stage. As shown in Fig. 4(e), the third time-of-flight measurement of PA signal t3 = 10.8 μs gave the next predicted depth information d4 = 8.1 mm. The corresponding Raman spectrum was shown in Fig. 4(f). It was found that d4 = d3 (the error <0.11 μs with 5-MHz transducer used) indicating the depth prediction was converged, and the maximum PA and Raman responses were achieved very fast in only 3 steps. If using the conventional depth-resolved Raman/fluorescence spectroscopy method by linearly successive searching, it requires at least 80 scanning

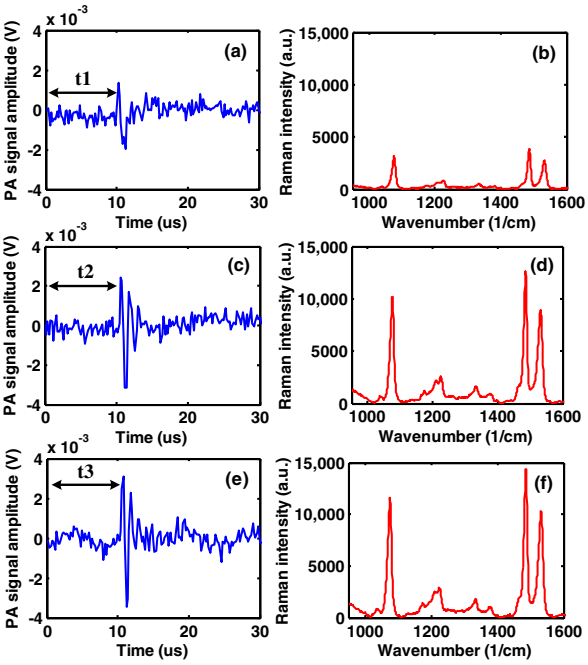

Fig. 4. PA-guided Raman spectroscopy measurement results. Recorded PA signal and Raman signal amplitudes at positions: (a) and (b) d1 = 0 mm; (c) and (d) d2 = 7.0 mm; (e) and (f) d3 = 8.1 mm.

steps to reach the maximized Raman response for an accuracy of 0.1 mm calculated by 8 mm/0.1 mm = 80 steps [17], the proposed PA-guided Raman spectroscopy approach could improve the operation speed significantly, depending on the targeted depth and scanning strategy, faster by >26 times (80/3 = 26.7) in this experiment.

The proposed PA-guided Raman spectroscopy approach attempts to utilize the correlation of both methods to achieve fast depth-resolved Raman measurement in an iterative way beyond the straightforward dual-modal PA-Raman combination approaches in previous literatures [18,19]. It is worth noting that although the proposed approach could provide the depth information for Raman measurement, the tight optical focusing in scattering medium is a significant and long-standing problem to be solved. In recent years, several interesting optical focusing techniques were reported to focus the light in scattering medium utilizing ultrasonic tagging and wavefront shaping [20,21]. Furthermore, utilizing PA signal as feedback to iteratively achieve the optimized optical focusing through wavefront shaping techniques has been reported [22–24]. It is expected that a seamlessly fusing of our proposed PA-guided Raman spectroscopy approach with the recent developed optical focusing techniques in scattering medium will render a further promising Raman spectroscopy diagnostic tool for real clinical applications, e.g., skin cancer detection, which is still an untapped area and deserves further development as our future work.

In conclusion, we have proposed PARS: a fast depth-resolved Raman spectroscopy technique based on photo-acoustic signal time-of-flight depth measurement and its strong correlation with Raman signals. After only several steps of iterative focusing, maximized Raman scattering signals could be detected by focusing the light accurately into the spot of the phantom with PA-signal-based depth measurement and guidance. Hence it could expedite the development of depth-resolved Raman spectroscopy technique toward skin and other deep cancer diagnostics with advanced wavefront-shaping-based optical focusing techniques.

[†]The authors contributed equally to this work.

Funding. Singapore Ministry of Health's National Medical Research Council; Singapore National Research Foundation (NMRC/EDG/1062/2012).

REFERENCES

1. E. B. Hanlon, R. Manoharan, T. W. Koo, K. E. Shafer, J. T. Motz, M. Fitzmaurice, J. R. Kramer, I. Itzkan, R. R. Dasari, and M. S. Feld, Phys. Med. Biol. **45**, R1 (2000).
2. P. J. Caspers, G. W. Lucassen, E. A. Carter, H. A. Bruining, and G. J. Puppels, J. Invest. Dermatol. **116**, 434 (2001).
3. R. Baker, P. Matousek, K. L. Ronayne, A. W. Parker, K. Rogers, and N. Stone, Analyst **132**, 48 (2007).
4. M. D. Morris, P. Matousek, M. Towrie, A. W. Parker, A. E. Goodship, and E. R. C. Draper, J. Biomed. Opt. **10**, 014014 (2005).
5. P. Matousek, I. P. Clark, E. R. C. Draper, M. D. Morris, A. E. Goodship, N. Everall, M. Towrie, W. F. Finney, and A. W. Parker, Appl. Spectrosc. **59**, 393 (2005).
6. L. H. V. Wang and S. Hu, Science **335**, 1458 (2012).
7. F. Gao, X. H. Feng, Y. J. Zheng, and C. D. Ohl, J. Biomed. Opt. **19**, 067006 (2014).
8. L. V. Wang, Nat. Photonics **3**, 503 (2009).
9. D. Razansky, M. Distel, C. Vinegoni, R. Ma, N. Perrimon, R. W. Koster, and V. Ntziachristos, Nat. Photonics **3**, 412 (2009).
10. H. F. Zhang, K. Maslov, G. Stoica, and L. H. V. Wang, Nat. Biotechnol. **24**, 848 (2006).
11. X. H. Feng, F. Gao, and Y. J. Zheng, Opt. Lett. **39**, 3414 (2014).
12. X. D. Wang, Y. J. Pang, G. Ku, X. Y. Xie, G. Stoica, and L. H. V. Wang, Nat. Biotechnol. **21**, 803 (2003).
13. F. Gao, X. H. Feng, and Y. J. Zheng, Appl. Phys. Lett. **104**, 213701 (2014).
14. V. V. Yakovlev, H. F. Zhang, G. D. Noojin, M. L. Denton, R. J. Thomas, and M. O. Scully, Proc. Natl. Acad. Sci. USA **107**, 20335 (2010).
15. V. V. Yakovlev, G. D. Noojin, M. L. Denton, B. A. Rockwell, and R. J. Thomas, Opt. Lett. **36**, 1233 (2011).
16. E. Salomatina, B. Jiang, J. Novak, and A. N. Yaroslavsky, J. Biomed. Opt. **11**, 064026 (2006).
17. Y. H. Ong and Q. Liu, Opt. Lett. **38**, 2647 (2013).
18. J. V. Jokerst, A. J. Cole, D. Van de Sompel, and S. S. Gambhir, ACS Nano **6**, 10366 (2012).
19. M. F. Kircher, A. de la Zerda, J. V. Jokerst, C. L. Zavaleta, P. J. Kempen, E. Mittra, K. Pitter, R. M. Huang, C. Campos, F. Habte, R. Sinclair, C. W. Brennan, I. K. Mellinghoff, E. C. Holland, and S. S. Gambhir, Nat. Med. **18**, 829 (2012).
20. X. A. Xu, H. L. Liu, and L. V. Wang, Nat. Photonics **5**, 154 (2011).
21. B. Judkewitz, Y. M. Wang, R. Horstmeyer, A. Mathy, and C. H. Yang, Nat. Photonics **7**, 300 (2013).
22. T. Chaigne, O. Katz, A. C. Boccara, M. Fink, E. Bossy, and S. Gigan, Nat. Photonics **8**, 59 (2014).
23. J. W. Tay, P. Lai, Y. Suzuki, and L. H. V. Wang, Sci. Rep. **4**, 3918 (2014).
24. P. X. Lai, L. D. Wang, J. W. Tay, and L. H. V. Wang, Nat. Photonics **9**, 126 (2015).